NASA DEVELOP National Program
California – Ames

Summer 2024

Clear Lake Volcanic Field Disasters

Creating a Deformation Record Using InSAR to Assess Hazards and Detect Volcanic Unrest in Clear Lake Volcanic Field

DEVELOP Technical Report

August 9th, 2024

Charles Nuncio (Project Lead)
Alexandra Crilley
Shilpa Kannan
Ivan Tochimani-Hernandez

Advisors:
Dr. Morgan Gilmour, NASA Ames Research Center (Science Advisor)
Dr. Mike Poland, USGS Yellowstone Volcano Observatory (Science Advisor)
Dr. Brianna Corsa, USGS California Volcano Observatory (Science Advisor)
Dr. Franz Meyer, University of Alaska Fairbanks & Alaska Satellite Facility (Science Advisor)
Lisa Tanh, ESRI (Science Advisor)

Lead:
Lauren Webster (California – Ames)

1. Abstract

Clear Lake Volcanic Field (CLVF) in northern California is at a high threat potential for volcanic hazards. Eruptions leading to increased seismic activity could result in silicic domes, cinder cones, and flows that would be dangerous to the residential areas near the volcanic field. Remotely sensed Earth observations can reveal volcanic processes in the subsurface, which are essential to the timely monitoring of potential volcanic activity. In particular, Sentinel-1 C-band Synthetic Aperture Radar (C-SAR) and Digital Elevation Model (DEM) data capture relative surface deformation at unprecedented high spatial and temporal resolutions. Leveraging C-SAR and DEMs, we conducted interferometric analysis from January 2016 to December 2023. Our results demonstrate 1) the mean surface displacement velocity of the CLVF is measured to undergo 5 to 10-centimeter scale deformation and shows a strong relationship with the surrounding faults, 2) apparent seasonal differences in rates of surface change, and 3) seismic activity associated with the geyser geothermal field has a strong association with cumulative surface displacement, with active fault zones having 2 to 5 cm of additional displacement. Results indicate that deformation is linked to deep pressure sources causing stresses on the surficial environment that should be considered in hazard mitigation. This study provides a baseline of historic deformation, aiding hazard analysts in communication efforts and streamlining decision-making for potential risks to region residents.

Key Terms

Remote Sensing, Deformation, Volcanic Field, Interferometric Synthetic Aperture Radar (InSAR), Sentinel-1 Satellite

2. Introduction

2.1 Background

The California Coast Range Mountains are home to many volcanoes that pose high threats to the state. While most are considered dormant, areas such as the Clear Lake Volcanic Field (CLVF) are susceptible to eruptions, ash, and debris flows that could damage agriculture systems and displace communities (Mangan et al., 2019). Clear Lake is specifically hazardous due to potential interaction between its magma chamber and the lake itself, which may result in explosive phreatomagmatic eruptions that could significantly impact northern California (Mangan, 2019). Due to this, it is critical to be able to understand and identify signals related to volcanic activity.

Before an eruption, chambers beneath volcanoes fill with increased pressure that leads to the ejection of magma and results in ground surface deformation. This ground movement and other volcanic signatures have been monitored through sensors that detect increased CO_2 emissions, slope angle, and seismic activity (Di Traglia et al., 2014). Recent studies have introduced the use of Interferometric Synthetic Aperture Radar (InSAR) as an additional volcano monitoring tool that compares two radar measurements of a location and returns a relative change in ground elevation (Pepe and Calò, 2017). This method has proven effective in observing upward ground motion (inflation) prior to eruption and downward deflation afterwards (Rivera et al., 2016).

The direction of deformation observed is largely dependent on the type of magma system present. Volcanoes may be classified as closed-vent magma systems, where gas emissions are trapped in the surface and thus result in observable ground inflation. In contrast, they may also be classified as open-vent volcanic magma systems, characterized by gas that can freely escape and where deformation may rarely be detected (Dzurisin et al., 2019). Closed vent systems, such as the one at CLVF, are at risk of experiencing phreatomagmatic explosions due to magma interaction with groundwater.

Given that CLVF is considered a closed-vent magma system, an InSAR time-series was proposed to track changes in deformation rates over time (Osmanoğlu et al., 2016). Deformation by itself, however, is not exclusive to volcanic activity; thus, additional methods were implemented to better distinguish volcanic deformation from atmospheric and surface-process signals. Such methods include Digital Elevation Models

(DEM) and land cover maps that inform us on absolute elevation and surface coverage respectively. Through this integrated approach, our team successfully created a historic baseline of volcanic deformation at CLVF. This method can be further applied to volcanic areas around the world for hazard assessment and disaster mitigation that more effectively protects communities at risk.

2.2 Project Partners & Objectives

We partnered with the United States Geological Survey (USGS) California Volcano Observatory, a division of the federal agency that is responsible for assessing hazards within the state's volcanic fields, including Clear Lake. This group investigates past eruptions and categorizes different volcanic hazards (Mangan et al., 2019). However, the observatory did not have a long-term record of deformation in the region prior to this project. Our project sought to assess the feasibility of using Sentinel-1 C-SAR data and Digital Elevation Models (DEMs) to create a historic time-series of deformation with InSAR analysis. By providing the USGS with a baseline of deformation for the CLVF, our end products can inform the decision-making process regarding future hazards, including eruptions, ash events, and debris flow that may threaten local communities. We also designed a creative communication series to help the USGS convey the importance of our research and illustrate potential risks to residents of the region.

2.3 Study Area and Period

Our area of interest is the Clear Lake Volcanic Field, the youngest and northernmost volcanic site within the California Coastal Range (Figure 1). To investigate this site, we retrieved InSAR data from the Alaska Satellite Facility (ASF) between January 1st, 2016, and December 31st, 2023. Consecutive interferograms were available for the four seasons across these years. We consider this period to be sufficient in establishing a baseline for the USGS to consult in future decision-making processes.

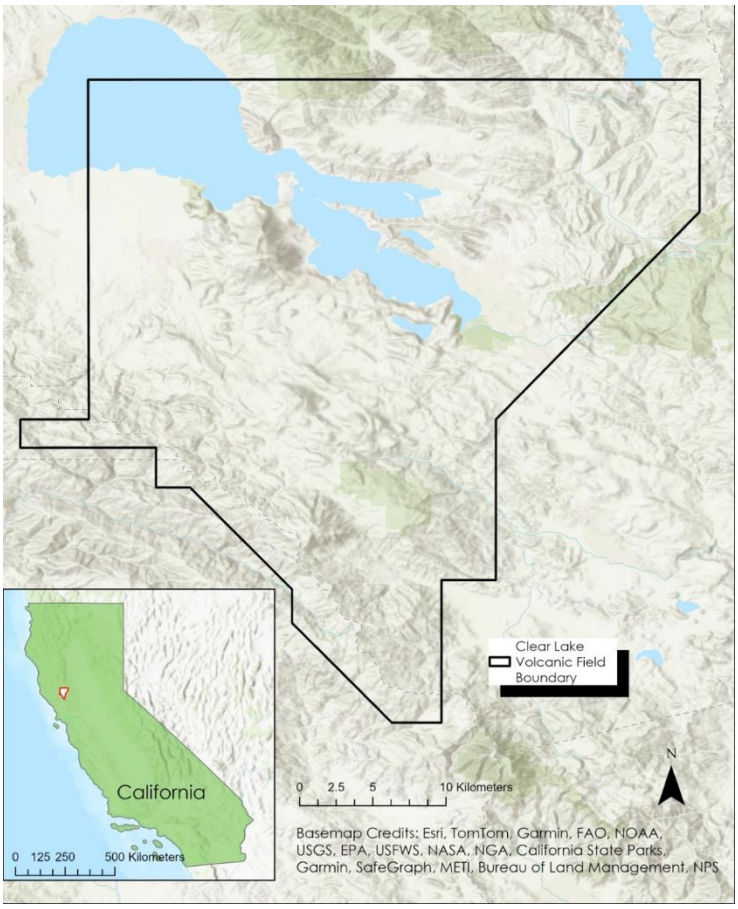


Figure 1. Study area boundaries within the Clear Lake Volcanic Field in Lake County, CA, USA.

3. Methodology

3.1. Data Acquisition

We used several forms of Earth observation data to understand the deformation at CLVF (Table 1). We started with the Sentinel-1 C-band Synthetic Aperture Radar (C-SAR) data, provided by the European Space Agency, to acquire elevation and vertical displacement data across the CLVF study area. We acquired our C-SAR data through the Alaska Satellite Facility (ASF) from NASA's Earth Science collection. Additionally, we obtained Sentinel-5P TROPOMI Sulfur Dioxide data from the Google Earth Engine (GEE) data catalog. Finally, we collected Aqua MODIS land surface temperature measurements from the GEE data catalog. We included the USGS 3D Elevation Program (3DEP) Digital Elevation Models (DEM), and the MERIT global hydrology digital elevation dataset obtained through GEE's data catalog as ancillary datasets (Table 2; U.S. Geological Survey, 2023). Finally, we procured a visual image collection from the Landsat 8 collection, which was also available on GEE's data catalog (U.S. Geological Survey, 2020). We collected datasets for all extracted parameters between January 2016 and December 2023, totaling seven years.

Table 1
Earth observations acquired for this study

Sensor/Satellite	Parameters	Processing Level	Provider
Sentinel-1	Synthetic Aperture Radar C-Band	Ground Range Detected, log scaling	European Space Agency
Landsat 8 OLI	Visible Bands	Level 2, Collection 2, Tier 1	USGS Earth Explorer
Aqua MODIS	Land Surface Temperature	Daily Global, 1km	National Aeronautics and Space Administration
Sentinel-5P TROPOMI	SO_2 Column Density	Near Real-Time	European Space Agency

Table 2
Ancillary datasets acquired for this study

Data	Parameters	Processing Level	Provider
USGS 3DEP	Digital Elevation Model	10m, 1/3 Arc-Second	United States Geologic Survey
MERIT Hydro	Digital Elevation Model	90m, 3 Arc-Second	Global Hydrology Group
National Land Cover Database	Land Cover	2021 Release	United States Geologic Survey
USGS Earthquake Catalog	Earthquake Magnitude >2.5	Near Real-Time	United States Geologic Survey
CHIRPS	Precipitation	Near Present, mm/d	University of California Santa Barbara

3.2 Data Processing

We developed two types of time-series to understand the deformation history of the CLVF. The first was an InSAR time-series that evaluated relative ground displacement based on phase difference between two measurements. Similarly, we produced a Digital Elevation Model (DEM) time-series that returned absolute displacement and was calculated directly from elevation differences. Additionally, we created a land cover map to aid in accounting for possible errors from heavily vegetated areas that could affect the interferogram data.

3.2.1 InSAR Time-Series

We retrieved unwrapped interferograms from the Alaska Satellite Facility's Vertex data portal and subsequently processed them using the OpenSARLab workflow. OpenSARLab utilizes the Miami InSAR time-series software (MintPy), which follows stacking workflow procedures as defined by Yunjun et al. (2019; Figure 2). We executed MintPy's workflow sequentially in two phases: correcting unwrapping errors and inverting for a phase time-series. The inverted phase was corrected for additional noise such as tropospheric delay, phase de-ramping, and topographic residuals, which can occur when radar data are collected by the satellite. MintPy incorporates outside inputs such as global atmospheric correction models and DEMs to address errors noted in the time series. MintPy reprocessed our interferogram data, taking into account noise corrections through multiple geophysical inversion iterations, until it was deemed viable for a displacement time-series. We then used this displacement time-series for surface velocity estimations for the volcanic field.

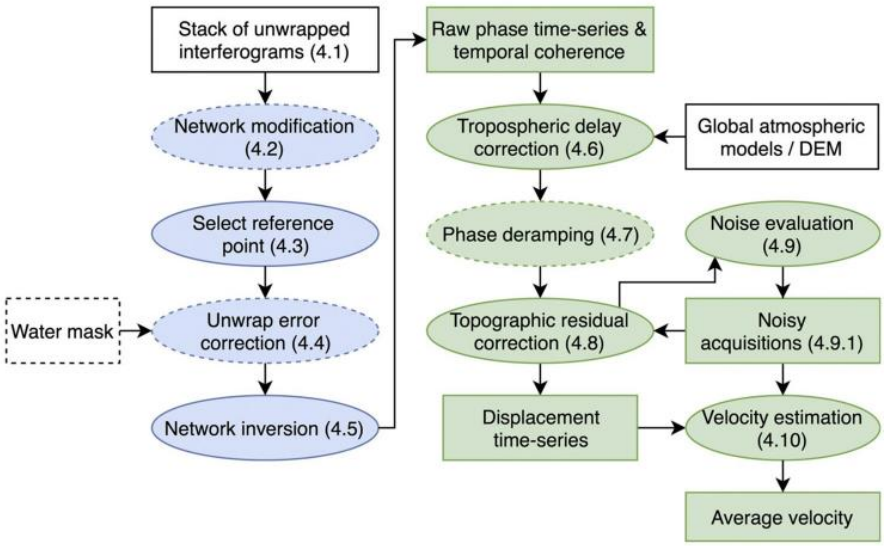


Figure 2. MintPy's workflow procedures. This represents the fourth sub-process within the plan provided by OpenSarLab. Blue steps show unwrapping-error corrections, and green steps show noise correction for displacement time-series development (Yunjun et al., 2019).

3.2.2 DEM Time-Series and Land Cover Map

We produced a DEM time-series and land cover map to aid in InSAR interpretations at CLVF.
The DEM time-series was posed as an "absolute" elevation change reference for the InSAR's "relative" change, while we used a land cover map to better understand potential decorrelating effects of local vegetation. We retrieved 90m resolution data from the MERIT global hydrology data set (Yamazaki et al., 2019) for January 1st, 2014, to January 1st, 2024. We extracted elevation data and applied a mask to interpolate for no-data value points. We then calculated and compared the mean elevations of CLVF for every month, tracking elevation change in a time-series.

We used an in-house NASA DEVELOP Google Earth Engine script to produce the land cover map. This script utilized machine learning, trained with the 2021 National Land Cover Database (NLCD) dataset, to

classify Landsat 8 true color data. Output classifications included dry land, forest, other vegetation, developed land, and water (Dewitz, 2021).

3.3 Data Analysis

3.3.1 InSAR Displacement Maps

We visually interpreted seasonal InSAR displacement maps over 2016–2023 in the OpenSARLab program. We determined the boundaries for each seasonal period by following meteorological season guidelines that outline temperature-cycle based three-month groupings (NOAA, 2024). Specifically, we selected the initial start date as the first available interferogram recognized by ASF-Vertex, while the end date ensured the last interferogram retrieved did not go past seasonal boundaries (Table 3). For this specific analysis, this consistent classification method was the most efficient and reduced opportunities for error.

Table 3

Seasonal Data Parameters

Season	Start Date (First Day of Month)	End Date (Last Day of Month)
Winter	December 1st	February 29th
Spring	March 1st	May 31st
Summer	June 1st	August 31st
Fall	September 1st	November 30th

Alongside these time-span parameters, we used ascending data at a 24-day baseline, manually connected the data points sequentially, set an overlap threshold of 50%, and selected a 20x4 output within ASF-Vertex's filtration system. Furthermore, we manually deleted incomplete interferogram data, adjusted the coherence threshold to 0.6, and used default parameters for tropospheric delay corrections and masking processing when proceeding with the OpenSARLab MintPy analysis. After visually interpreting deformation patterns modeled by OpenSARLab within these parameters, we then conducted further investigation on land surface temperature, earthquake magnitude, SO_2 concentrations, precipitation, and land cover data.

3.3.2 Land Surface Temperature using Aqua MODIS Data

Land surface temperature can be used to identify changes in near-surface magma chamber activity. Using Google Earth Engine and Aqua MODIS data, we analyzed nighttime land surface temperature from 2016–2023 to determine if thermal signatures related to the magma chamber could be identified. The resulting data indicated that there were seasonal changes in temperature that show noticeable peaks in the summer months and are the lowest during the winter months. However, these readings were consistent throughout the entire timespan, indicating that the magma chamber's thermal signatures were not identified within the data.

3.3.3 Earthquake Magnitude using USGS Earthquake Catalog & SO_2 using Sentinel-5P TROPOMI

We evaluated earthquake magnitude data at a monthly rate from 2016 to 2023 using data from the USGS Earthquake Catalog. Earthquake magnitude is considered an indicator for volcanism due to the potential result of magma intruding through the faults. It is also essential to note that earthquakes may not be necessarily associated with magmatic activity but could be the result of tectonic movement. We also assessed sulfur dioxide (SO_2) data from Sentinel-5P TROPOMI to determine if a change in seepage through these faults could indicate the movement of magma and associated gasses. We examined the mean SO_2 content at a monthly scale, for the years 2019 through 2023. By comparing these two parameters at a monthly scale, the team determined seasonal relationships between seismicity, SO_2, and deformation.

3.3.4 Precipitation using CHIRPS & Landcover using National Land Cover Database

We investigated Climate Hazards InfraRed Precipitation with Station Data (CHIRPS) data related to precipitation and landcover data from the National Land Cover Database to determine if the deformation changes being observed are primarily volcanic or other environmental factors in the system, such as mass

wasting events. We plotted seasonal precipitation using GEE and visualized the five land cover classes in GEE in an effort to identify deformation associated with water movement.

4. Results & Discussion

4.1 Analysis of Results

Through evaluating our InSAR time-series, we identified seasonal trends in deformation at the CLVF. In addition to the 2016–2023 seasonal time-series, we further subdivided each season into 2–3-year intervals to recognize short-term deformation events (Figure 3). From this analysis, we found that deformation varied between seasons; with greater displacement detected in the summer and winter, and milder in the spring and fall. This variability directly mirrors regional data that show there is higher relative precipitation in the winter and lower in the summer (Figure 4). Increased water content often results in mass wasting, while a decrease may lead to destabilization. This is observed as a large contrast between subsidence and uplift.

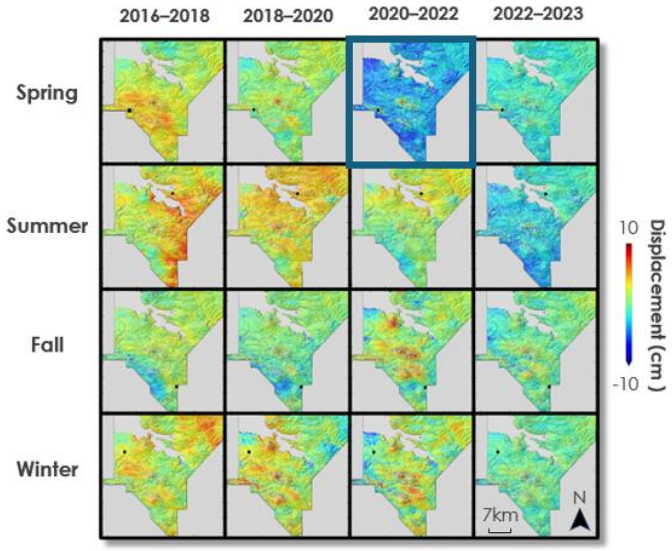


Figure 3. Seasonal deformation differences at the Clear Lake Volcanic Field. The spring 2020–2022 deformation map is considered an outlier with abnormally heavy subsidence (blue box).

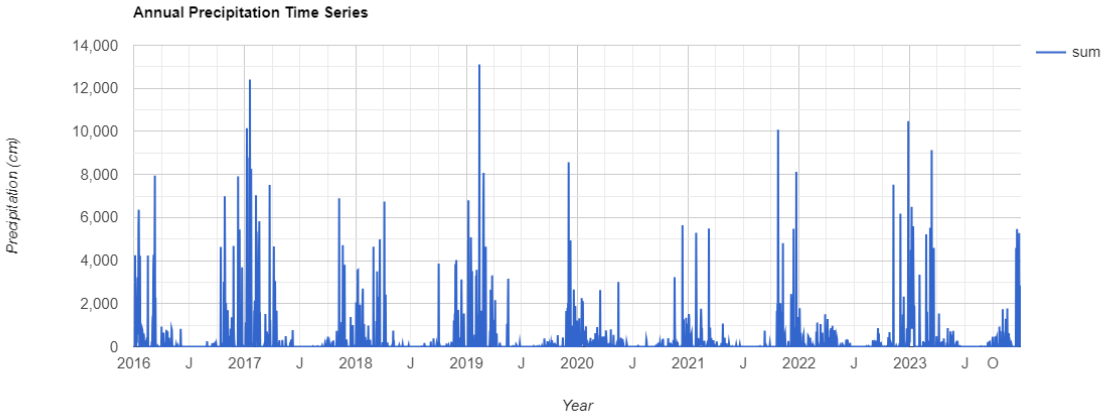


Figure 4. Annual total precipitation within the Clear Lake Volcanic Field.

Further trends include a noticeable difference in deformation direction between the early and late time-series. Uplift was predominant in the earlier intervals, while significantly greater subsidence is observed in the later years. Thorough local analysis behind this difference was outside the scope of this study; however, regional precipitation events may have influenced the observed deformation. One example was a large atmospheric river in January 2021 that hit the northwestern United States that introduced major rainfall, leading to increased erosion. This subsidence can be specifically seen in the Spring 2020–2022 deformation map (blue box), where subsidence is significantly large compared to other seasonal time intervals.

While we successfully identified seasonal and temporal InSAR trends, supplemental data sets showed no correlation between volcanism and observed deformation. The land cover maps that we produced served as analog for groundwater fluctuations (Figure A1; Figure A2). Because levels of vegetation remained consistent throughout the study, we inferred that groundwater changes were miniscule and therefore did not contribute to deformation changes. Other reference methods included evaluating land surface temperature to check for potential thermal signatures representative of magma chambers (Figure A3). From this, higher temperatures were consistently detected in the summer compared to the winter, showing no indication of additional thermal influences. This observation is consistent with previous literature that notes that surface deformation is difficult to detect if the magma chamber is below a depth of 5 km, as per the case of the CLVF's 6–15 km deep magma source (Mitchell et al., 2023).

We saw little association between the deformation time-series and volcanic indicators, such as earthquake magnitude and SO_2 levels. USGS Earthquake Catalog data show that three magnitude 5.0+ earthquakes were recorded near the study area from 2016–2023. When cross-referencing these three events to the short-term interval deformation maps, we found little relation. Additional magnitude 3.5–4.0 earthquakes were recorded during our study period; however, they were designated as background noise due to their frequent occurrence. SO_2 measurements similarly showed no relation between major earthquake events and ground deformation (Figure 5; Figure A4; Figure A5). As such, there is little evidence for volcanic deformation at the CLVF.

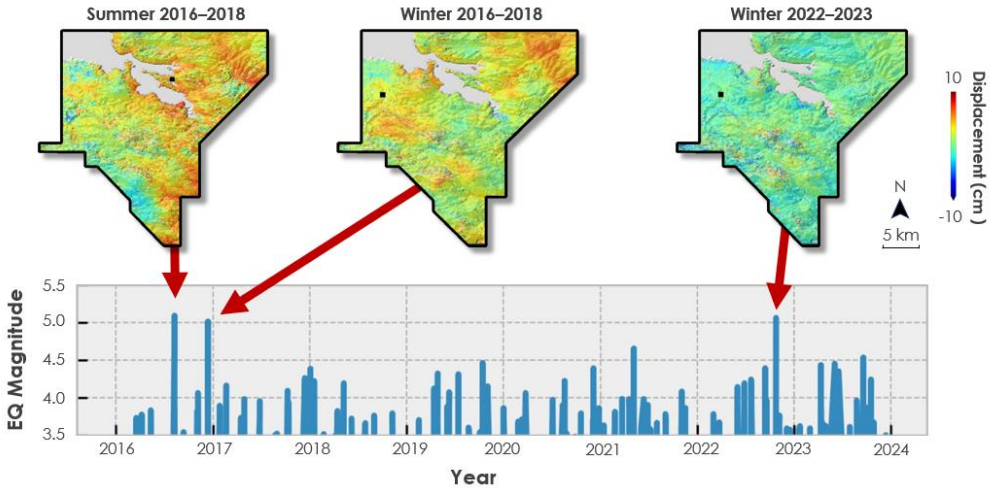


Figure 5. Earthquake magnitude data and deformation observations at the Clear Lake Volcanic Field.

4.2 Errors & Uncertainties

We encountered errors such as less coherent satellite data, coarse elevation data, atmospheric distortion, and temporal omissions. The satellite data that we chose used a 24-day baseline and allowed us to widen the timespan for seasonal analysis; however, it reduced the data coherence. Furthermore, coarse elevation data and temporal omissions from 90 and 10-meter resolution respectively did not allow for time-series analysis with the DEM mapping products (Figure A6). Lastly, we had to remove data with too much atmospheric

distortion, resulting in timespan gaps within our InSAR processing workflow. Hence, errors related to data availability issues and distortion resulted in reduced data quality and hindered deeper analysis.

4.3 Feasibility & Partner Implementation

We found that it was feasible to apply an InSAR-based deformation record using MintPy to contribute to USGS's decision making needs. This product serves as a baseline of deformation for our partners to use to better detect and analyze future volcanic hazard events. However, we did not find the DEM time-series to be a useful method for our research study area due to low resolution data. The InSAR deformation time-series, however, can overcome the low-resolution data and provide immense benefit to our partners. This provides necessary historical geographic data of Clear Lake Volcanic Field needed to better mitigate future occurrences of volcanic hazards.

5. Conclusions

We determined it is feasible to use Sentinel-1 C-SAR data to detect ground deformation at Clear Lake Volcanic Field. By retrieving InSAR data from the Alaska Satellite Facility's Vertex platform and processing it through the MintPy workflow, we successfully produced deformation maps for all four seasons between 2016–2023. We identified that there was a considerable amount of deformation within the volcanic field based on our time-series. We also observed notable differences in surface displacement across seasons, warranting further investigation into potential confounding environmental variables. After cross-referencing our InSAR data analysis with supplemental maps, we concluded that observed uplift and subsidence are predominantly associated with tectonic activity. There was limited evidence suggesting that deformation would be due to volcanic activity within the study area. While our results did not indicate current or projected volcanic activity at CLVF, our end products and supplementary maps will still be of use to our partners at the USGS California Volcano Observatory. The InSAR time-series maps our team created will serve as a baseline of deformation for the region that allows the USGS to more effectively detect future hazards.

6. Acknowledgements

Thank you to the following individuals for supporting our project this summer:

- Lauren Webster (NASA DEVELOP Node Lead – Ames)
- Maya Hall (NASA DEVELOP Impact Analysis Fellow)
- Dr. Morgan Gilmour, NASA Ames Research Center
- Dr. Mike Poland, USGS Yellowstone Volcano Observatory
- Dr. Brianna Corsa, USGS California Volcano Observatory
- Dr. Jessica Ball, USGS California Volcano Observatory
- Dr. Seth Burgess, USGS California Volcano Observatory
- Jonathan Stock, USGS National Innovation Center
- Dr. Franz Meyer, University of Alaska Fairbanks & Alaska Satellite Facility
- Lisa Tanh, ESRI

This material contains modified Copernicus Sentinel data (2024), processed by ESA. Any opinions, findings, and conclusions or recommendations expressed in this material are those of the author(s) and do not necessarily reflect the views of the National Aeronautics and Space Administration. This material is based upon work supported by NASA through contract 80LARC23FA024.

7. Glossary

Deformation – the upwards (uplift) or downwards (subsidence) movement of Earth's crust in a specific location, potentially related to volcanic activity deep below the surface.
DEM – Digital Elevation Model, a virtual representation of a landscape highlighting various topographic features.
Earth observations – satellites and sensors that collect information about the Earth's physical, chemical, and biological systems over space and time.
Geothermal field – region in which the Earth's surface is naturally warmed by intrusions or magma activity deep underground. The Geysers geothermal field is the largest in the world and overlaps with our study site.
InSAR – Interferometric Synthetic Aperture Radar, a remote sensing technique that utilizes satellite data to detect deformation of Earth's surface. InSAR data is collected by comparing two different radar images of the same area taken at different times from a similar point in space. The two images are then combined to create a single wavelength-revealing surface topography.
MintPy – Python workflow used to process InSAR data and generate deformation time-series maps.
MODIS – Moderate Resolution Imaging Spectroradiometer, a satellite-based sensor for monitoring Earth science data, operated by NASA. We are using Aqua MODIS data, launched in 2002.
Phase deramping – a step in processing InSAR data that involves "cleaning" signals, using a reference point to identify absolute differences between frequencies.
Scoria Cone – a cinder cone, a common type of volcano formed by an explosive eruption at the volcanic vent.
Sentinel-1 – the first satellite of the Copernicus program conducted by the European Space Agency. Includes C-band radar, which we are using in this research.
Topographic residuals – signal errors caused by inaccuracies in digital elevation models.
Tropospheric delay – time effects to InSAR imagery that occur when the radar signal passes through the troposphere, must be corrected during processing to determine the accurate results.

8. References

Ball, J. (2022). Stratigraphy and eruption history of maars in the Clear Lake Volcanic Field, California. Frontiers in Earth Science, 10. https://doi.org/10.3389/feart.2022.911129

Copernicus Sentinel data 2014-2024. Retrieved from ASF DAAC June 21, 2024, processed by ESA.

Copernicus Sentinel-5P (processed by ESA), 2020, TROPOMI Level 2 Sulphur Dioxide Total Column. Version 02. European Space Agency. https://doi.org/10.5270/S5P-74eidii

Dewitz, J., 2023, National Land Cover Database (NLCD) 2021 Products: U.S. Geological Survey data release, https://doi.org/10.5066/P9JZ7AO3.

Di Traglia, F., Nolesini, T., Intrieri, E., Mugnai, F., Lev, D., Rosi, M., & Casagli, N. (2014). Review of ten years of volcano deformations recorded by the ground-based InSAR monitoring system at Stromboli volcano: a tool to mitigate volcano flan dynamics and intense volcanic activity. Earth-Science Reviews, 139, 317-335. https://doi.org/10.1016/j.earscirev.2014.09.011

Dzurisin, D., Lu, Z., Poland, M., & Wicks, C. (2019). Space-Based Imaging Radar Studies of U.S. Volcanoes. Frontiers in Earth Science, 6, https://doi.org/10.3389/feart.2018.00249

Mangan, M., Ball, J., Wood, N., Jones, J.L., Peters, J., Abdollahian, N., Dinitz, L., Blankenheim, S., Fenton, J., and Pridmore, C. (2019). California's exposure to volcanic hazards. United States Geological Survey, Volcano Science Center.

Mitchell, M. A., Peacock, J. R., & Burgess, S. D. (2023). Imaging the magmatic plumbing of the Clear Lake Volcanic Field using 3-D gravity inversions. Journal of Volcanology and Geothermal Research, 435, 0377-0273, https://doi.org/10.1016/j.jvolgeores.2023.107758

NOAA. (2024, March 22). Meteorological Versus Astronomical Seasons. National Centers for Environmental Information (NCEI). https://www.ncei.noaa.gov/news/meteorological-versus-astronomical-seasons

Osmanoğlu, B., Sunar, S., Wdowinski, S., Cabral-Cano, E. (2016). Time series analysis of InSAR data: Methods and trends. ISPRS Journal of Photogrammetry and Remote Sensing, 115, 0924-2716, https://doi.org/10.1016/j.isprsjprs.2015.10.003

Pepe, A., & Calò, F. (2017). A Review of Interferometric Synthetic Aperature RADAR (InSAR) Multi-Track Approaches for the Retrieval of Earth's Surface Displacements. Applied Sciences, 7, 1264. https://doi.org/10.3390/app7121264

Rivera, A. M., Amelung, F., & Mothes, P. (2016). Volcano deformation survey over the Northern and Central Andes with ALOS InSAR time series. Geochemistry, Geophysics, Geosystems, 17, 2869-2883. https://doi.org/10.1002/2016GC006393

U.S. Geological Survey Earth Resources Observation and Science Center. (2020). Landsat 8 OLI/TIRS [Dataset]. US Geological Survey. https://doi.org/10.5066/f78s4mzj

U.S. Geological Survey, 2023, 3D Elevation Program 1-Meter Resolution Digital Elevation Model, accessed June 21, 2024 at URL https://www.usgs.gov/the-national-map-data-delivery

Wan, Z., Hook, S., Hulley, G. (2021). MODIS/Terra Land Surface Temperature/Emissivity Daily L3 Global 1km SIN Grid V061. NASA EOSDIS Land Processes Distributed Active Archive Center. Accessed

2024-07-31 from https://doi.org/10.5067/MODIS/MOD11A1.061 Water Resources Research, vol.55, pp.5053-5073, 2019, doi: 10.1029/2019WR024873

Yamazaki, D., Ikeshima, D., Sosa, J., Bates, P.D., Allen, G.H., & Pavelsky, T.M. (2019). A high-resolution global hydrography map based on latest topography datasets. Water Resources Research, 55, 5053-5073. https://doi.org/10.1029/2019WR024873

Yunjun, Z., Fattahi, H., & Amelung, F. (2019) Small baseline InSAR time series analysis: Unwrapping error correction and noise reduction. Computers & Geosciences, 133, https://doi.org/10.1016/j.cageo.2019.104331

9. Appendix

Appendix A: *Supplemental Figures*

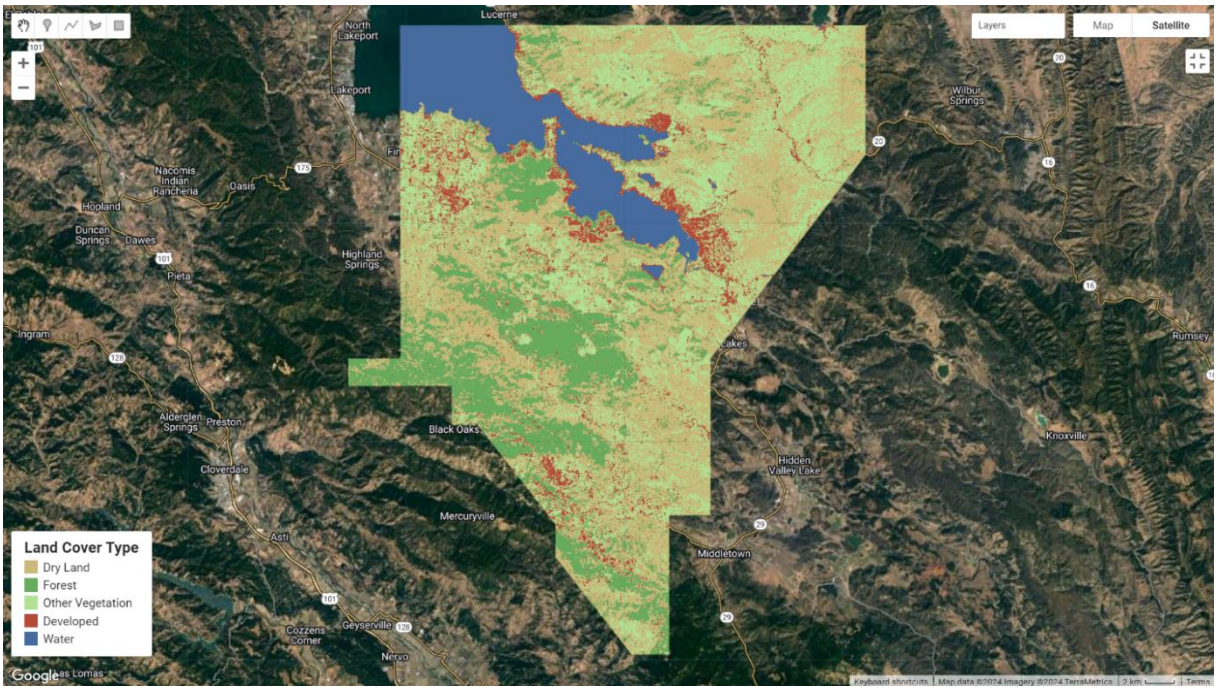


Figure A1. Land cover map for Clear Lake Volcanic Field in the year 2021.

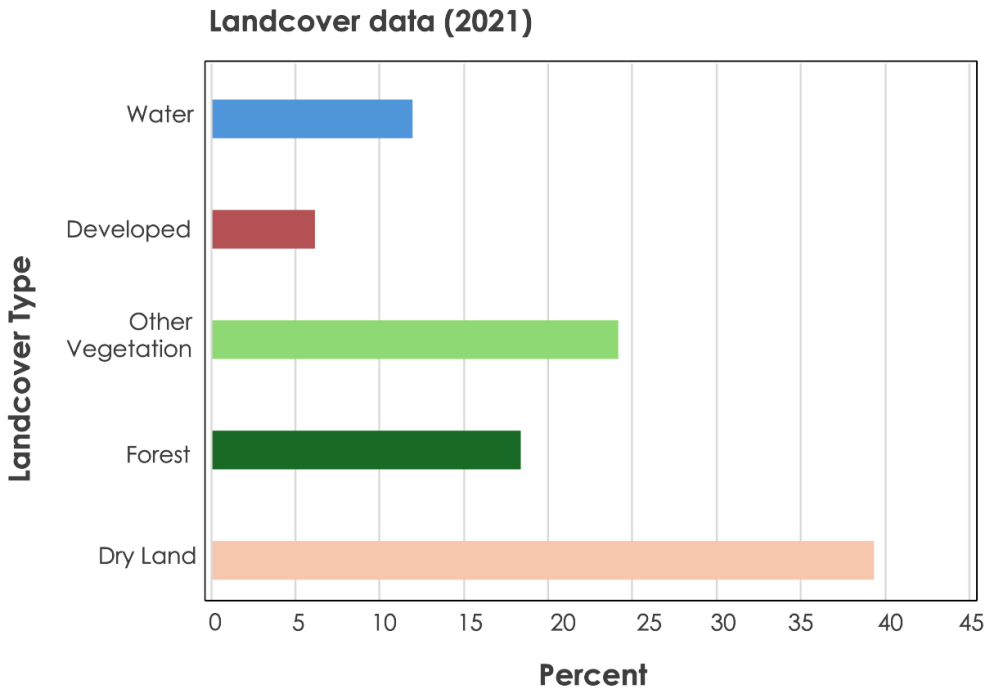


Figure A2. Land cover type percentage within the Clear Lake Volcanic Field study area in the year 2021.

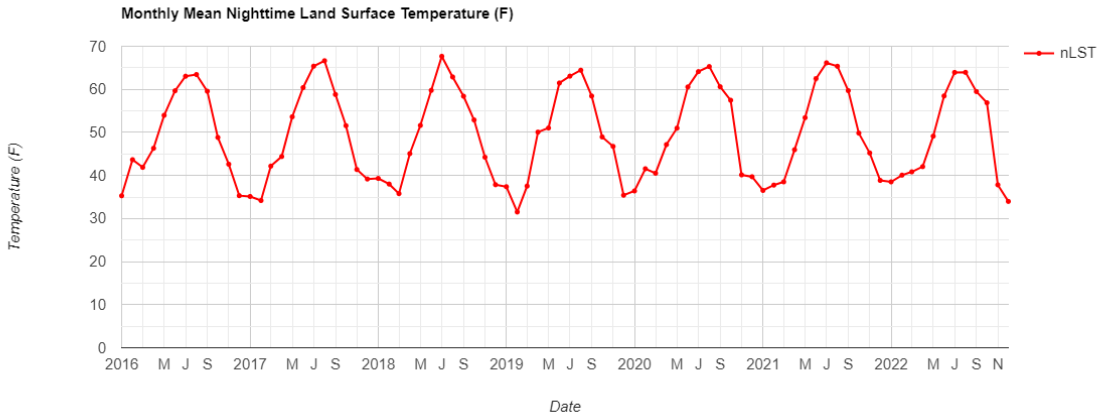


Figure A3. Land surface temperature time-series for Clear Lake Volcanic Field from 2016–2023.

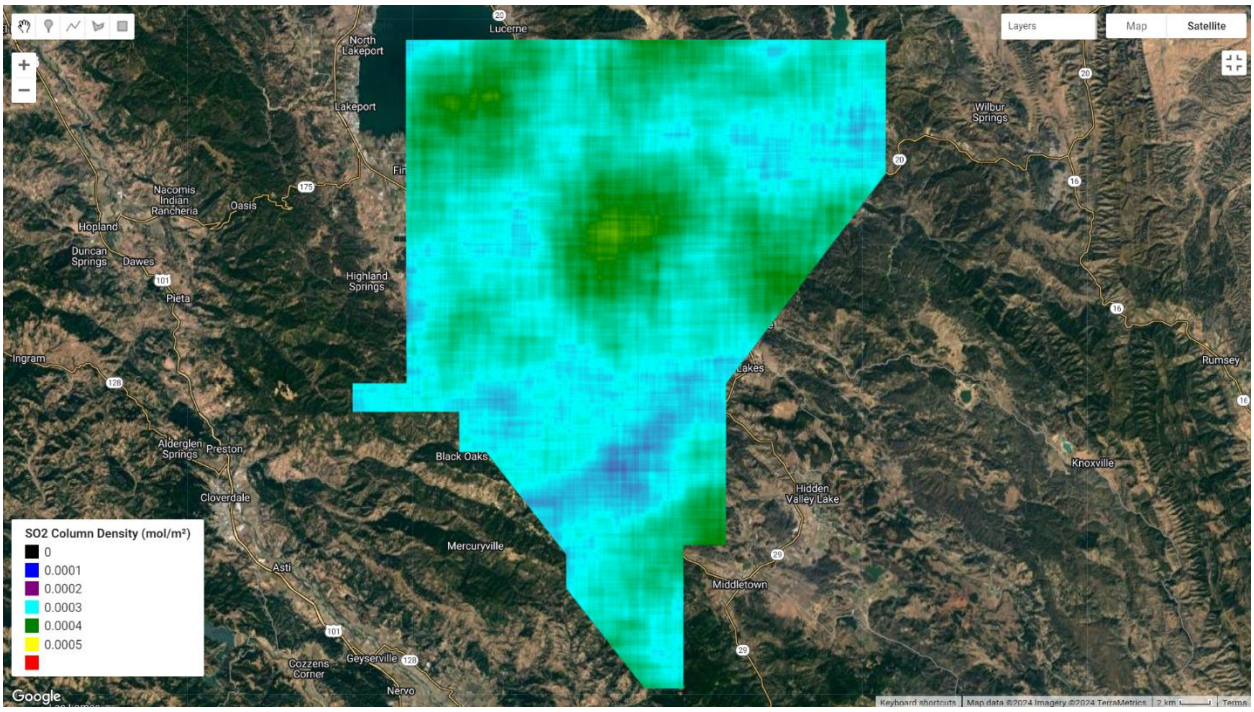


Figure A4. Sulfur dioxide column density map for Clear Lake Volcanic Field in the year 2021.

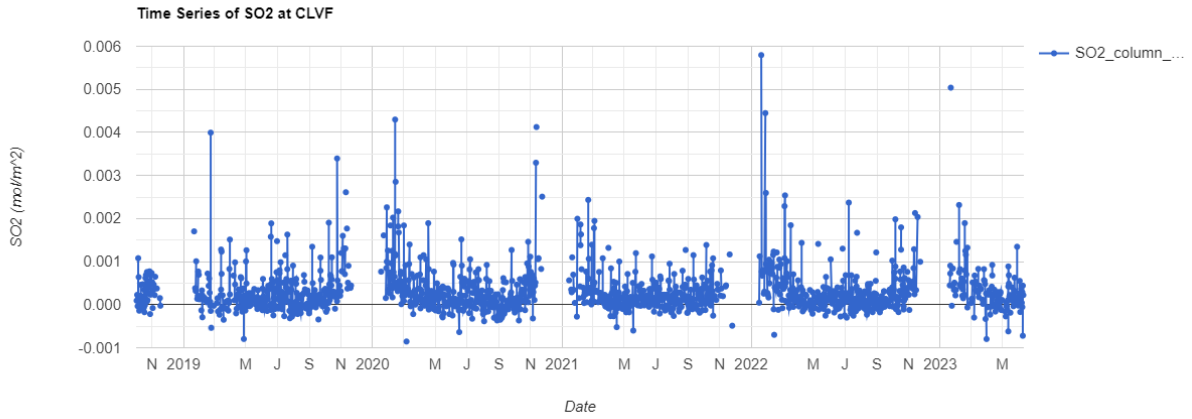


Figure A5. Sulfur dioxide column density values for Clear Lake Volcanic Field from 2019 to 2023.

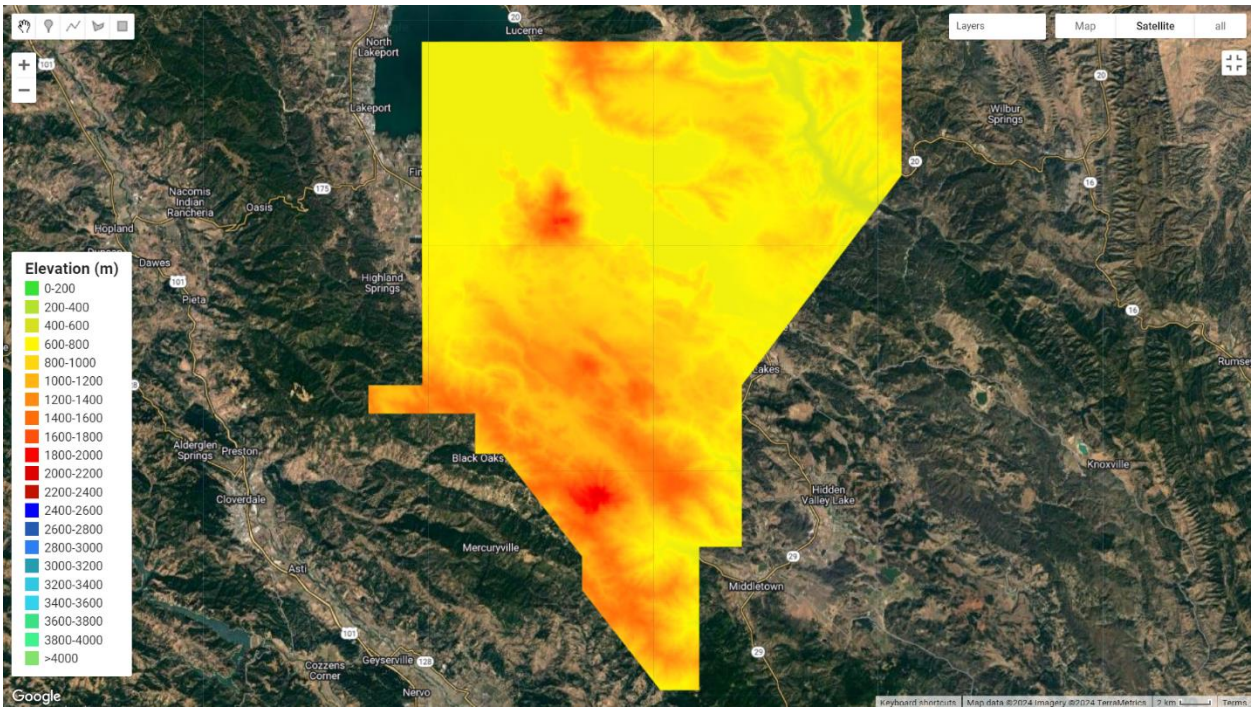


Figure A6. Digital elevation model map for Clear Lake Volcanic Field in the year 2021.